Image Cover Sheet

CLASSIFICATION	SYSTEM NUMBER
UNCLASSIFIED	516321

TITLE

Vicarious calibration of airborne hyperspectral sensors in operational environments

System Number:

Patron Number:

Requester:

Notes:

DSIS Use only:

Deliver to: CL

This page is left blank

This page is left blank

ELSEVIER

Remote Sensing of Environment 76 (2001) 81–92

Remote Sensing of Environment

www.elsevier.com/locate/rse

Vicarious calibration of airborne hyperspectral sensors in operational environments

Jeff Secker[a,*], Karl Staenz[b], Robert P. Gauthier[b], Paul Budkewitsch[b]

[a]Defense Research Establishment Ottawa (DREO) Ottawa, Ontario, Canada K1A 0Z4
[b]Canada Centre for Remote Sensing, 588 Booth Street, Ottawa, Ontario, Canada K1A 0Y7

Received 2 March 2000; received in revised form 26 September 2000; accepted 27 September 2000

Abstract

A reflectance-based vicarious calibration (RBVC) method has been used to correct the radiometric coefficients for hyperspectral data obtained with the Probe 1 sensor over the Raglan region of northern Quebec, and to perform a radiance renormalisation for compact airborne spectrographic imager (*casi*) data obtained over Goose Bay, Labrador. It relies on the simultaneous acquisition of ground-based reflectance spectra for at least one calibration site within the hyperspectral flight line. The RBVC method yields a new set of radiometric coefficients that convert the hyperspectral data from digital numbers (DNs) to radiances, and that are applicable to flight lines taken under different conditions. For both the Raglan and the Goose Bay projects, the calibration site was a gravel airstrip, and ground-based reflectance measurements were made with a GER3700 field spectrometer using a Spectralon panel for reference. This represents a novel use of the RBVC method for validation and correction of the sensor's radiometric calibration at the time of data acquisition, applied in an operational setting that lacks a large, bright and homogeneous calibration target and well-characterized atmospheric conditions. Analysis of the errors involved in correcting the radiometric coefficients yielded a total relative error (averaged over wavelength) of 3.9–5.6% on the final reflectance spectra.

Keywords: Vicarious calibration; Hyperspectral data; Field spectrometer; Atmospheric correction; *casi*; Probe 1; GER3700

1. Introduction

The sensors used to acquire airborne hyperspectral data, such as airborne visible/infrared imaging spectrometer (AVIRIS, Vane et al., 1993), compact airborne spectrographic imager (*casi*, Anger et al., 1996, Babey & Anger, 1989), SWIR full spectrum imager (SFSI, Neville, Rowlands, Marois, & Powell, 1995) and Probe 1 are complex optomechanical devices. During their transport, installation and operation, these sensors can be subjected to significant stresses. If these stresses occur between the laboratory calibration and the overflight, and if any minute misalignments occur as a result, then it is possible that the laboratory calibration (both spectral registration and radiometric coefficients) will not be appropriate to data acquired during the overflight. If this occurs, the errors in the calibration will not be detected until the data have been acquired and a preliminary analysis has been performed.

Vicarious calibration provides a method for the absolute calibration of remote sensing sensors via reference to accurate spectral measurements made separately from the airborne sensor. This is an absolute calibration method that yields a new set of radiometric coefficients that can be used to replace those derived in the laboratory (Dinguirard & Slater, 1999, Slater et al., 1987).

With the *reflectance-based* vicarious calibration (RBVC) method, the at-sensor radiometric data are calibrated by comparison against accurate ground-based measurements for a target located within the overflight area. The RBVC method is most often discussed in the context of satellite sensors as a method to monitor the radiometric calibration (Markham, Barker, Slater, & Biggar, 1997, Slater et al., 1987, Teillet et al., 1990, Thome et al., 1998, Thome, Markham, Barker, Slater, & Biggar, 1997). As well, it provides a useful and necessary way to monitor and verify the calibration coefficients for airborne hyperspectral data, and it has been used in this capacity for AVIRIS

* Corresponding author. Tel.: +1-613-993-2859; fax: +990-8906.
E-mail address: jeff.secker@dreo.dnd.ca (J. Secker).

0034-4257/00/$ – see front matter
PII: S0034-4257(00)00194-2

(Green, Conel, Margolis, Chovit, & Faust, 1996, Vane et al., 1993). While the vicarious calibration of AVIRIS data performs well under ideal conditions, these conditions are not always met during the course of hyperspectral surveys, and the RBVC method must be evaluated for use in operational environments.

In truly operational settings, the accuracy of the vicarious calibration is reduced considerably due to several factors: (a) the difficulty inherent in locating a sufficiently large and homogeneous target within the overflight path (in fact this may not be possible); (b) the practical limitations on the number of ground-based reflectance measurements that can be made to characterize the calibration target, and (c) an inability to fully characterize the atmospheric conditions at time of overflight. However, provided that there is simultaneous acquisition of field spectra for an area within the overflight path, the RBVC method can be used successfully with the additional advantage that *the calibration is performed at the time of the data acquisition*.

In this paper an implementation of the RBVC method for hyperspectral data is described, the result of which is a corrected set of radiometric coefficients. This is an iterative numerical technique that adjusts the radiometric coefficients to reduce the absolute difference between the ground-based (calibrating) reflectance spectrum and the reflectance spectrum extracted from the hyperspectral data to within a specified tolerance. This method is implemented in the imaging spectrometer and data analysis system (ISDAS, Staenz, Szeredi, & Schwarz, 1998) software developed at the Canada Centre for Remote Sensing (CCRS).

This methodology has been applied to two different hyperspectral data sets obtained in northern Canada, both of which required corrections to the radiometric coefficients. These are: 128-band Probe 1 data obtained near Raglan Lake on the eastern end of the Cape Smith fold belt in northern Quebec, and 72-band *casi* data obtained near Goose Bay, Labrador. The objective of the Raglan project is to use hyperspectral and ground-based data together with spectral unmixing techniques to create mineral maps of the exposed rock in this barren region of northern Quebec (Staenz, Nadeau, Secker, & Budkewitsch, 2000). For the Goose Bay project, the *casi* hyperspectral data will be used to establish a land-use baseline prior to flooding of the lower Churchhill river (Pollock et al., 2000). In both cases, ground-based reflectance data were obtained simultaneously with the overflight using a field spectrometer.

2. Ground-based data acquisition and preprocessing

Field research done in support of the Raglan and Goose Bay hyperspectral projects included the acquisition of ground-based reflectance spectra using the GER3700 portable field spectrometer, which has 704 channels spanning the wavelength interval between 350 and 2490 nm. For each of these studies, the field spectrometer was configured with a 10° field of view (FOV) lens, giving a 0.26-m diameter ground FOV from a height of 1.5 m.

The Kattiniq–Donaldson airstrip, located within the Probe 1 flight line, was chosen as the calibration site for the Raglan project. The airstrip is surfaced with glacial drift, a mixture of clay, sand, and gravel packed together, which to the eye appears as a homogeneous mixture of the constituent materials on a scale of a few meters. The GER3700 was used to obtain six reflectance spectra of the airstrip surface about 35 min after the overflight. The atmospheric conditions were stable during the intervening time, and the sky was clear with no cirrus clouds visible during the measurement period.

The airstrip in North West River (north of the Innu community of Sheshatshiu) was chosen as the calibration site for the Goose Bay project. The airstrip surface consists of a mixture of sand and gravel, which on a scale of a few meters appeared homogeneous to the eye. The GER3700 was used to obtain 27 reflectance spectra for the airstrip's surface. These were made simultaneously with the *casi* overflight. It was a clear day with stable atmospheric conditions. During this time, measurements of the atmospheric water vapour content, U_{H_2O}, and the aerosol optical depth, $\delta_a(550\ \text{nm})$ — were made using a Microtops II sunphotometer. The average values were $\delta_a(550\ \text{nm}) = 0.043$ and $U_{H_2O} = 1.47\ \text{g/cm}^2$.

The raw spectra acquired with the field spectrometer were converted to reflectance using scans of a Spectralon reference panel, and these were then preprocessed to correct for angular and spectral variations in the reflectance of the Spectralon panel. The angular variations — the bidirectional reflectance factor (BRF) — are due to deviations from a Lambertian surface. The spectral variations refer to wavelength variations in the spectral reflectance factor (SRF).

Letting L denote the raw radiance measured from the reference Spectralon panel, and with $R(\theta,\lambda)$ and $S(\lambda)$ referring to the BRF and the SRF functions, respectively, then L_{ref} refers to the corrected reference radiance, given by [Eq. (1)]

$$L_{\text{ref}}(\lambda)_i = \frac{R(\theta_i,\lambda)L(\lambda)_i}{S(\lambda)}, \tag{1}$$

where θ is the solar zenith angle (SZA) and λ is the wavelength. Then the mean reflectance ρ_{targ} for N measurements of the same target is given in percent by [Eq. (2)]

$$\rho_{\text{targ}} = \sum_{i=1}^{N} \frac{100 L_{\text{targ}}(\lambda)_i}{L_{\text{ref}}(\lambda)_i} \tag{2}$$

The correction factors $R(\theta,\lambda)$ and $S(\lambda)$ were determined by measuring the Spectralon reference panel at the University of Arizona's Optical Sciences Center in March 1999, and values at the appropriate angle and wavelength were obtained via interpolation. Finally, the corrected reflectance spectra were averaged to yield a single mean corrected reflectance spectrum for each of the calibration sites, which were then convolved to the band centres for the appropriate

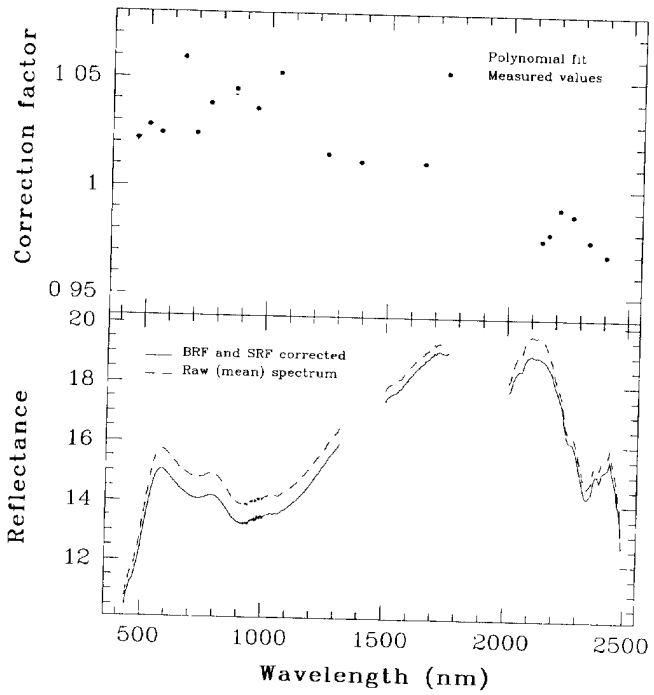

Fig 1 (Upper panel) A polynomial fit to the measured correction values (combining the angular and spectral variations) for a solar zenith angle (SZA) of $\theta = 43.0°$ (Lower panel) The effect of the correction factor is illustrated using the mean GER3700 field reflectance spectrum for the Raglan calibration site

hyperspectral sensor It is these spectra against which the airborne hyperspectral data are calibrated

In Fig 1, this correction process is illustrated for the field data obtained on the Kattiniq–Donaldson (Raglan) airstrip. In the upper panel, the dotted line illustrates the fourth-order polynomial fit to the measured correction values (combining the angular and spectral variations) for an SZA of $\theta = 43.0°$ The RMS deviation of the measured values from the polynomial fit is less than ± 0.01, yielding a relative uncertainty of less than 1% in the corrected field reflectance spectra In the lower panel, the effect of this correction factor is illustrated using the mean GER3700 field reflectance spectrum for the Raglan calibration site It results in a maximum absolute difference between the raw and the corrected spectra of $\simeq$0.73% near 790 nm The regions around the broad atmospheric water vapour absorption features (1380 and 1900 nm) are masked out, and the noise near 1000 nm is due to the decreased sensitivity of the Si and PbS detectors at the limits of their ranges.

For both of these data sets, the standard deviation at each wavelength (σ) for the corrected reflectance spectra was calculated and used to derive the standard error on the mean reflectance spectrum, given by $\sigma/\sqrt{N}$, where N represents the number of corrected field spectra averaged together An average of this relative standard error over the wavelength range relevant to the hyperspectral sensor yields values of 4.0% in the visible and near-infrared (VNIR) and 3.7% in the shortwave infrared (SWIR) for the Kattiniq–Donaldson airstrip, versus 1.3% in the VNIR for the North West River airstrip The decrease in standard error for the North West River airstrip is due primarily to the number of measurements averaged (i.e., 27 vs 6) and the $1/\sqrt{N}$ dependence of the standard error It may also be attributed in part to a difference in homogeneity of the airstrip surface composition

3. Airborne hyperspectral data

3.1 Data acquisition

The hyperspectral data for the Raglan project was obtained with the Probe 1 sensor in July 1998 (Table 1) The Probe 1 is a high signal-to-noise sensor with 128 spectral bands spanning the wavelength range from 440 to 2500 nm, with bandwidths between 11 and 22 nm full width at half maximum (FWHM). It is a whiskbroom scanner with four linear 32-element detectors, a Si photodiode detector for the 440–900 nm (VNIR) range, and three InSb detectors for the 900–1350 nm (NIR), 1390–1800 nm (SWIR1) and 1980–2500 nm (SWIR2) ranges. The Probe 1 instrument has 12-bit digitisation, and a 60° FOV, which for the altitude of this mission corresponds to a swath width of about 4.5 km and 7.5 m × 7.5 m pixels. The Probe 1 sensor is mounted on a three-axis gyrostabilized platform that compensates for the effects of the aircraft motion for up to ±5° for each axis. The hyperspectral data are delivered as raw data (digital numbers, DNs), along with the radiometric coefficients and the spectral registration information that were determined via laboratory calibration.

The hyperspectral data for the Goose Bay project was obtained with the *casi* sensor (Anger et al., 1996) along a north–south flight line over the communities of North West River and Sheshatshiu. For this mission, the *casi* was configured for 72 bands in the range 400 to 950 nm, with bandwidths of $\simeq$8.7 nm FWHM The FOV for *casi* is 35.6°, which at the altitude flown for this mission yields 4 m × 4 m pixels The *casi* data are delivered with units of radiance, scaled by a factor of 10^3 and truncated to integer.

Table 1
Parameters for the atmospheric correction of the Raglan Probe 1 data

Date	1998-07-28
GMT	17 00 00
Latitude	61°40′26″N
Longitude	73°29′09″W
Sensor altitude	3.69 km (ASL)
Atmospheric model	Subarctic summer
Aerosol model	Continental (rural)
Solar zenith angle	42.76°
Solar azimuth angle	179.86°
Terrain elevation	0.47 km (ASL)
Water vapour content	1.00 g/cm^2
Ozone column	0.346 cm atm
CO_2 mixing ratio	357.5 ppm
Visibility	50 km

ASL = above sea level

Table 2
Parameters for the atmospheric correction of the Goose Bay *casi* data

Date	1999-07-11
GMT	19 30 28
Latitude	53°23′19″N
Longitude	60°09′30″W
Sensor altitude	3 11 km (ASL)
Atmospheric model	Midlatitude summer
Aerosol model	Maritime
Solar zenith angle	49 57°
Solar azimuth angle	251 35°
Terrain elevation	0 03 km (ASL)
Water vapour content	1 47 g/cm^2
Ozone column	0 319 cm atm
CO_2 mixing ratio	357 5 ppm
Aerosol optical depth (at 550 nm)	0 043

3 2 *Preprocessing and atmospheric correction*

The Probe 1 raw data were dark subtracted and converted to radiance using the laboratory radiometric coefficients provided with the data The *casi* radiance data were scaled by a factor of 10^{-3} and then corrected to remove the effects of the aircraft roll For both the Probe 1 and *casi* sensors, the band centre wavelengths and bandwidths used initially were those derived in the laboratory calibration

The raw at-sensor radiance spectra were converted to surface reflectance via an atmospheric correction using the MODTRAN3 radiative transfer (RT) code (Anderson, Wong, & Chetwynd, 1995, Berk, Berstein, & Robertson, 1989) as implemented in the imaging spectrometer data analysis system (ISDAS) (Staenz & Williams, 1997) Inputs to MODTRAN3 include mission-specific and sensor-specific parameters, and model-specific choices for atmospheric properties. These are summarized in Table 1 (Probe 1) and Table 2 (*casi*). Due to the lack of a digital elevation model, a mean terrain elevation was used in each case.

For the Probe 1 data, the atmospheric water vapour content, U_{H_2O}, was estimated using a method that models the combined strength of the 940- and 1130-nm water vapour absorption lines in the spectra (Gao & Goetz, 1990, Green, Conel, Margolis, Brugge, & Hoover, 1991, Staenz & Williams, 1997) Inspection of pixels scattered throughout the image showed that the variation in atmospheric water vapour content was small ($\Delta U_{H_2O} = \pm 0\ 05$ g/cm^2), and an average value of $U_{H_2O} = 1\ 00$ g/cm^2 was used across the entire scene

3 3 *Correcting the spectroscopic calibration*

Small errors in the spectral registration of the hyperspectral sensor are not easily detected when viewing the radiance spectra Thus, the behaviour of the corrected surface reflectance spectra is analyzed in the vicinity of strong atmospheric absorption features This is an iterative process (Fig 2) in which small shifts are applied to the band centres specified in the spectral calibration, with the magnitude and sign estimated by inspecting the profile of the atmospheric absorption lines in the reflectance spectrum.

Specifically, the raw spectrum (DN) corresponding to a spatially averaged region was extracted from the image cube and converted to radiance using the radiometric and spectroscopic calibration derived in the laboratory This radiance spectrum was then corrected to surface reflectance using the MODTRAN3 RT code, as described in the previous section The results of a spectral misregistration are then visible in the reflectance spectrum as a characteristic over- and under-correction of atmospheric absorption features (Fig 3).

For the Probe 1 data, this process was applied separately for each of the four spectrometers, using the 760-nm O_2 line, the 820-, 940- and 1130-nm H_2O lines, and the SWIR CO_2 lines near 2005 and 2055 nm For the *casi* data, the 760-nm O_2 and the 820-nm H_2O lines were used Then, the wavelength shifts were calculated that best corrected the reflectance to obtain a smooth spectrum in the vicinity of these absorption features. With this technique, spectral shifts on the order of $\lesssim 0\ 5$ nm can be detected and corrected

3 4 *Extraction of target spectra and comparison with ground-based spectra*

In both the Probe 1 and *casi* cases, the airstrip calibration site was located within the hyperspectral scene visually, by

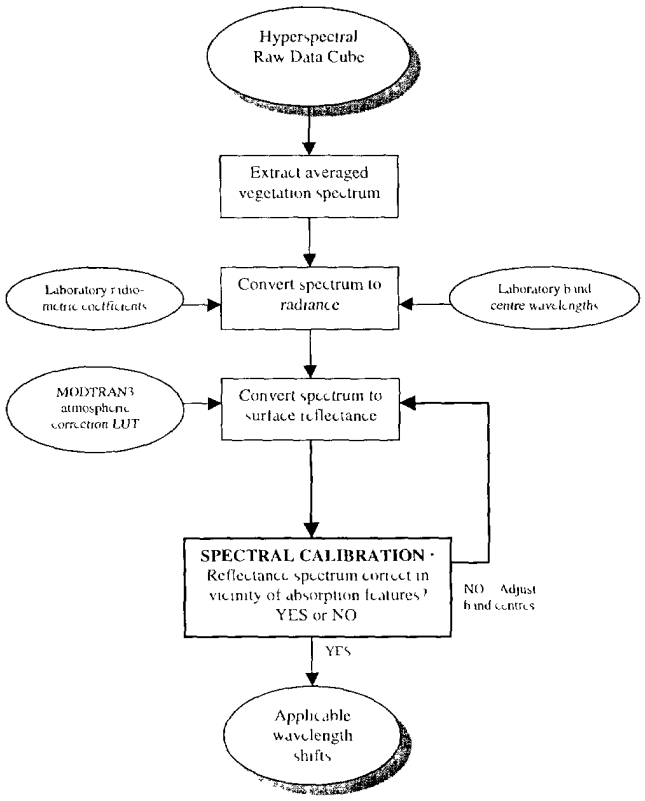

Fig 2 Data processing flow diagram for estimation of the wavelength shifts required to correct the spectral calibration of hyperspectral sensors (LUT = look-up table)

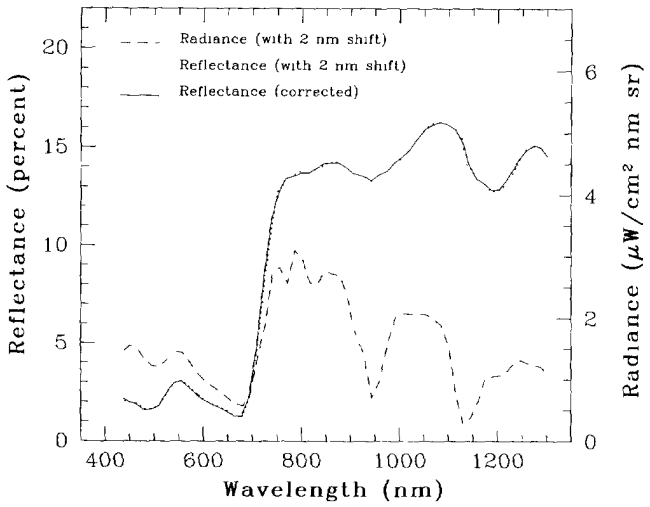

Fig 3 The effect on the reflectance spectrum of a 2-nm wavelength shift in the spectral calibration

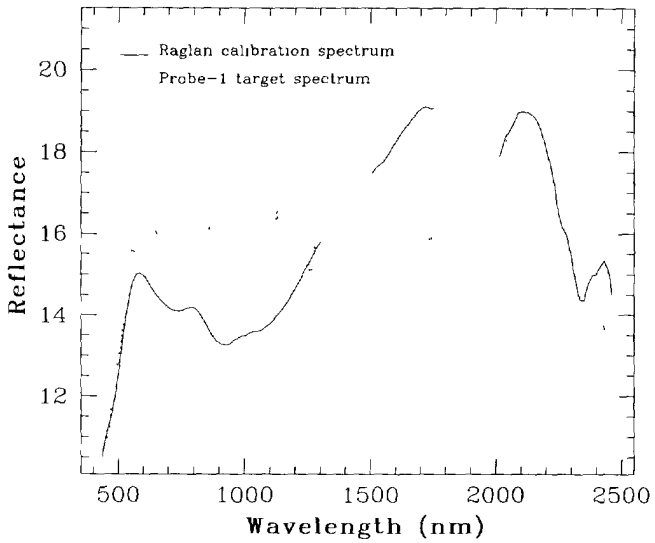

Fig 4 The calibrating (field) reflectance spectrum for the Raglan airstrip (solid line) compared with the Probe 1 reflectance spectrum for this site (dashed line)

comparing field notes with the airstrip boundaries and buildings or vehicles. These locations are accurate to within a few 10s of meters, but the location of individual field measurements cannot be correlated with single pixels in the scene, as the ground sites do not have differential GPS information, and because the airborne data are not georectified.

For the vicarious calibration it must be certain that these calibration sites are homogeneous and that the areas identified within the hyperspectral scenes include the ground calibration sites To this end, a region 12 pixels × 10 pixels in size (about 90 m × 75 m) was selected for the Probe 1 data, and a region 3 pixels × 12 pixels (about 12 m × 48 m) in size was selected for the *casi* data In both cases, the selected region is centred around the visually located calibration site, and the total area is sufficient to enclose the ground measurements

The spectra for the pixels in these regions were extracted from the hyperspectral data and averaged to yield a single mean reflectance spectrum for each of the Probe 1 and *casi* data Then, to test for homogeneity of the calibration sites, each of the calibration regions were subdivided into four adjacent subregions and the average reflectance spectra for each of these were compared with the average spectrum of the total region In both the Probe 1 and *casi* cases, the subregion spectra are all very similar in shape and amplitude, and they are all within one standard deviation of the average spectrum for the full region. Therefore, using an average spectrum derived from the full region will not adversely affect the comparison between the airborne data and the field data or the subsequent vicarious calibration As well, these separate regions can then be used to estimate the uncertainty associated with surface inhomogeneity and our inability to correlate the location of individual field measurements with single pixels in the Probe 1 scene

In Fig. 4, the mean Probe 1 reflectance spectrum for the 12 pixel × 10 pixel region (dashed line) is compared to the mean resampled GER3700 field reflectance spectrum (solid line). In the range 1500 nm$\lesssim\lambda\lesssim$1800 nm, the coefficients are significantly underestimated. In the range 550 nm$\lesssim\lambda\lesssim$1200 nm, the coefficients are greatly overestimated in general, and there are significant errors on a band-to-band basis that give rise to oscillations in the reflectance spectrum. The relative errors in the Probe 1 reflectance spectrum are between 10% and 18%. The

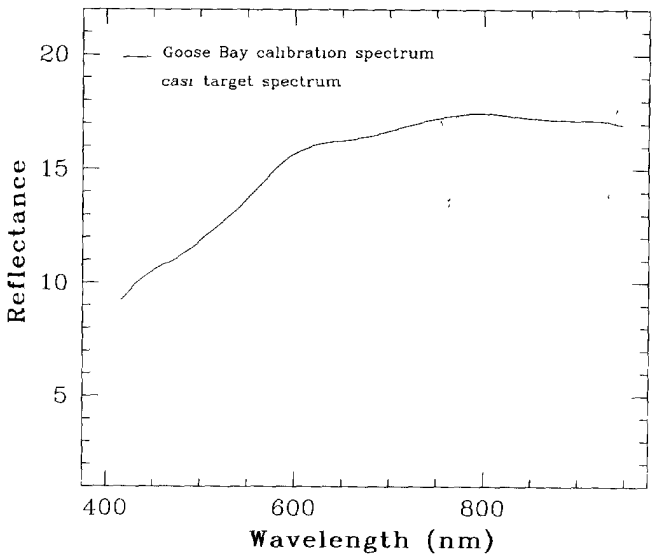

Fig 5 The calibrating (field) reflectance spectrum for the North West River airstrip (solid line) compared with the *casi* reflectance spectrum for this site (dashed line)

difference between these two spectra will be used as the basis for the vicarious calibration of the Probe 1 sensor.

In Fig. 5, the mean *casi* reflectance spectrum for the 3 pixel × 12 pixel region (dashed line) is compared to the mean resampled GER3700 field reflectance spectrum (solid line). The primary concerns with the *casi* data are (a) the decrease in sensitivity below a wavelength of ≃500 nm, and (b) the fact that the RT code with the appropriate parameters and models did not correctly compensate for the 760 nm O_2 absorption feature, even after the spectral shift was applied to the band centres. Note that the spikes above 925 nm are most likely noise resulting from a combination of reduced sensitivity of the Silicon detector, and a weak signal due to this water vapour absorption region. The difference between these two spectra will be used to renormalize the radiance calibration of the *casi* data.

4. Methodology and results

4.1. Reflectance-based vicarious calibration

The RBVC method as implemented in ISDAS is illustrated in Fig. 6. Vertically down the right side, the processing flow for the *field reflectance spectra* is illustrated. The left side illustrates the processing flow for the *airborne hyperspectral data*. The control module for the RBVC method is illustrated at the bottom centre. It takes as input the resampled mean field reflectance spectrum and the airborne hyperspectral reflectance spectrum for the calibration site, together with the initial values of the radiometric coefficients and a tolerance for matching of these spectra (absolute reflectance difference). Note that unlike the Probe 1 data, *casi* data are provided in units of radiance, so there are no radiometric coefficients to be

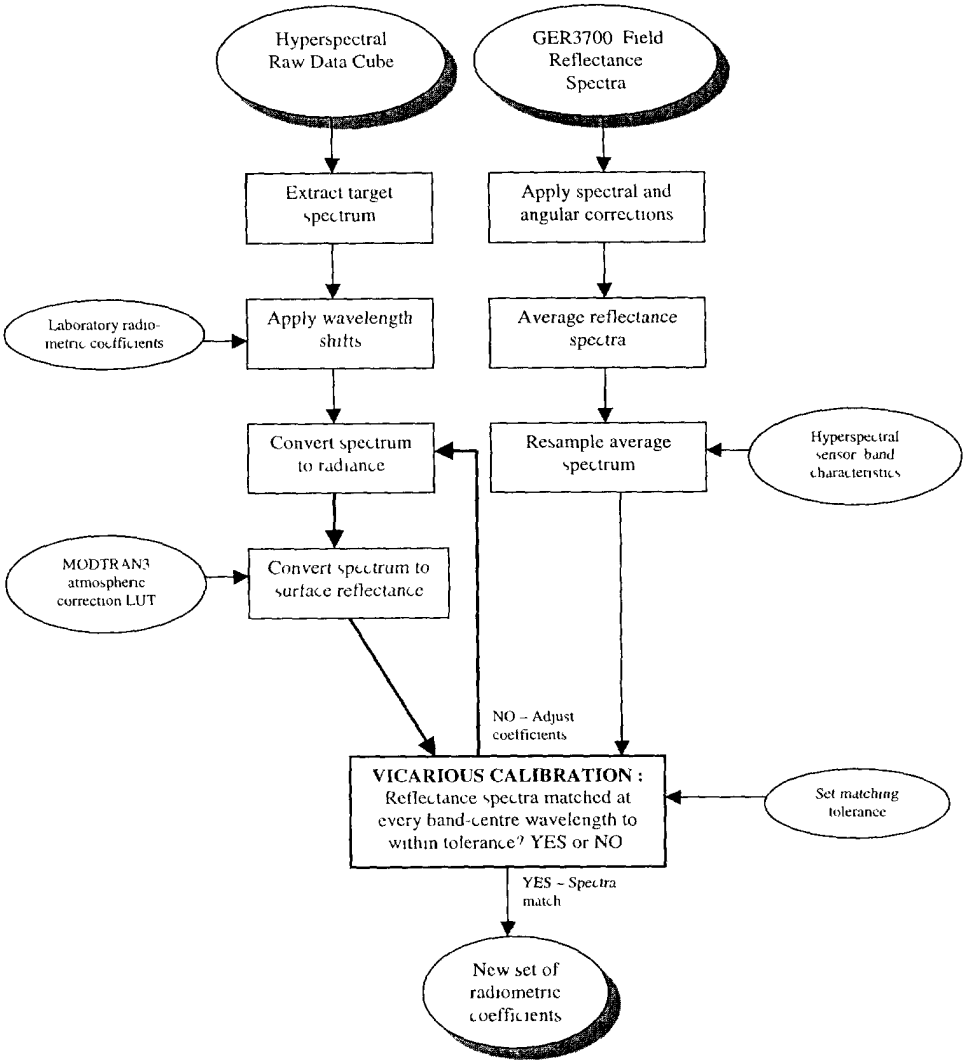

Fig. 6. Data processing flow diagram for the reflectance-based vicarious calibration (RBVC) method applied to airborne hyperspectral data in an operational setting.

adjusted However, the scaling factor of 10^{-3} that is applied to every band can be treated as a coefficient and subsequently the spectra can be renormalized as required

The RBVC control module uses an iterative numerical technique that adjusts the airborne sensor's radiometric coefficients to minimize the absolute reflectance difference between the two spectra This cycle of comparing the spectra and adjusting the radiometric coefficients in an incremental manner is repeated in subsequent iterations until the airborne hyperspectral reflectance spectrum agrees with the field reflectance spectrum to within the specified tolerance at each band Once these two spectra match, the control module terminates the iterative adjustment process, and the corrected set of radiometric coefficients are output.

An alternative and faster method that can be used to correct errors in the radiometric coefficients would be to calculate the scale factor that converts the DN directly to surface reflectance, by dividing the ground-based reflectance spectrum with the DN spectrum extracted from the hyperspectral data When applied to the hyperspectral scene as a whole, this yields surface reflectance without the need for explicit atmospheric correction However, this simple method has significant limitations, including, (a) the radiometric coefficients and radiance information are lost in the process, and (b) the derived coefficients are not applicable to data obtained under different atmospheric and/or observing parameters The advantage of the RBVC method implemented here is that it is not limited in either of these ways

4 2 Application to Probe 1 data

The mean Probe 1 reflectance spectrum and the mean resampled GER3700 spectrum were input to the vicarious calibration module, together with the atmospheric correction look-up table (LUT) generated a priori using MODTRAN3 as implemented in ISDAS A matching tolerance of 0 02% (absolute reflectance) was specified This resulted in a set of corrected radiometric coefficients for the Probe 1 data These were applied to the Raglan data, and as well to a Probe 1 data set obtained 3 days later (July 31, 1998) over a densely forested region near Timmins, Ontario

In addition, the vicarious calibration module was used in the same manner to derive four separate sets of corrected coefficients for the Probe 1 data, using the spectra extracted from the four 3 pixels × 10 pixels subareas of the primary calibration region located on the airstrip The variability in these four sets of coefficients was used to estimate the error introduced by an uncertainty in the spatial registration of the calibration site within the hyperspectral image The standard error (percent relative error) on the mean value of the coefficients varied between about 0 8% and 2 1% over the full wavelength range, and an appropriate average value is ≃1 5%

Reflectance spectra extracted for targets of interest in the Raglan and Timmins Probe 1 scenes are illustrated in Fig 7. These include spectra for rock (peridotite) and

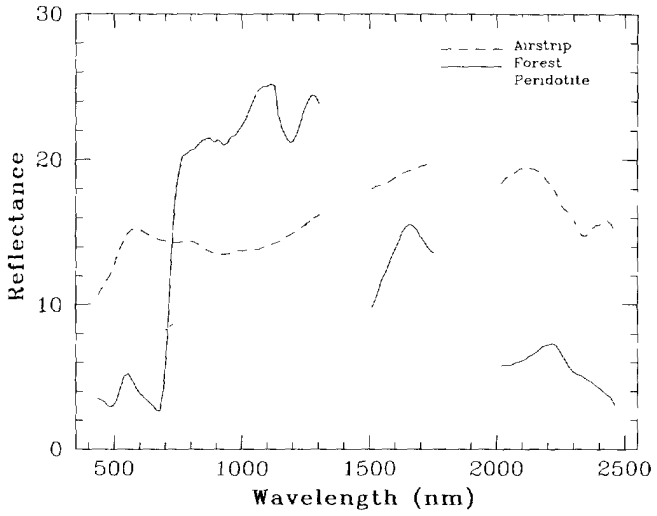

Fig 7 Probe 1 reflectance spectra resulting from the application of the corrected radiometric coefficients

the airstrip calibration target extracted from the Raglan scene, and a spectrum for a densely forested region from the Timmins scene Note that the Timmins scene was atmospherically corrected to surface reflectance using MODTRAN3 with mission and model parameters appropriate to this geographic region and atmospheric conditions For these targets, and in the wavelength regions corresponding to each spectrometer, the spectra exhibit markedly different characteristics (amplitude, shape, and absorption features), indicating that the RBVC method did not introduce any artifacts to the spectra and was successful for all spectrometers

4 3 Application to casi data

The mean spectrum for the airstrip extracted from the *casi* data, together with the mean resampled GER3700 field reflectance spectrum and the atmospheric correction LUT (generated a priori using MODTRAN3) were input into the vicarious calibration module, and the matching tolerance was set to 0.02% (absolute reflectance) This process modified the constant scaling factors of 0.001 specified for each band, resulting in a new set of values that differ for each band

The vicarious calibration module was used in the same manner to derive four sets of corrected scaling factors for the *casi* data using the spectra extracted from the four 3 pixels × 3 pixels subareas of the primary calibration site located on the airstrip The standard error varied between about 0 4% and 0 9%, and an appropriate average value over wavelength is ≃0 7% This standard error provides an estimate of the error introduced by an uncertainty in the spatial registration of the calibration site within the scene.

With the renormalisation of the *casi* data complete, reflectance spectra extracted for different targets in the

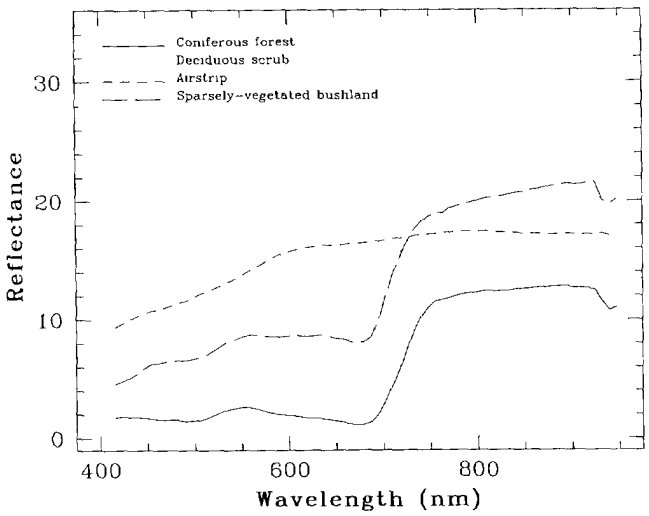

Fig. 8. *cont.* Reflectance spectra resulting from the radiance renormalisation.

scene are illustrated in Fig. 8. These include coniferous forest, deciduous scrub, sparsely vegetated bushland, with the airstrip calibration target provided for comparison. These renormalized spectra show a great improvement: the relative amplitudes between the visible and near-infrared are different for these spectra, as are their shapes, and the strength of the chlorophyll absorption at 680 nm varies considerably. Note that the drop in reflectance for $\lambda \gtrsim 925$ nm is due mainly to noise in the calibrating spectrum.

4.4. Validation using agricultural data

In July 1999, field measurements were made in support of Probe-1 hyperspectral data acquisition over Clinton, Ontario. This was an agricultural study, and at this time field reflectance spectra were obtained for crops, weeds, residue and soil. The RBVC method was used to correct the radiometric coefficients for this Probe-1 data, and the corrected coefficients were then applied to the rest of the data for subsequent analysis. This process is described below, along with the analysis of an independent target used to assess the validity of the RBVC method.

The calibration target used for the Clinton data was a patch of parched bare soil, 25 m × 25 m in size. It had been cleared of crop residue from the previous year, and was kept free of crop and weeds. The GER3700 field spectrometer was used to make three reflectance measurements of this soil patch, via reference scans of a Spectralon panel. A 3° lens was used from a height of 50 cm, yielding a 2.6-cm FOV. These spectra were corrected for the BRF and SRF effects, and the mean spectrum was resampled to the characteristics of the Probe-1 sensor.

The soil calibration patch was registered without ambiguity within the Probe-1 hyperspectral scene via visual inspection. The raw data (DN) spectrum for a single 5 m × 5 m pixel was extracted from the center of the soil patch, and converted to radiance using the laboratory calibration. For the atmospheric correction, a LUT was generated within ISDAS using MODTRAN3 (Section 3.2), with mission and model parameters appropriate to this geographic region and atmospheric conditions. The RBVC method was then used to generate a set of corrected radiometric coefficients that were applied to all of the Probe-1 hyperspectral data obtained during the Clinton study. Note that the field measurements of this calibration site were obtained two days prior to the overflight. However, the conditions were almost identical in terms of soil dryness, atmospheric conditions and sun angles, with no precipitation during the intervening two days.

For validation of the RBVC method, an independent target within the hyperspectral scene was selected. This is a 15 m × 40 m area of white beans that had been planted at double the normal density. The GER3700 with a 2.6-cm FOV was used to obtain five measurements of an optically thick stack of leaves from these plants, again via reference scans of the Spectralon panel. These spectra were corrected, averaged, and resampled to match the Probe-1 sensor, as was done for the field measurements of the dry soil patch.

The location of the double beans was registered without ambiguity within the Probe-1 hyperspectral scene via visual inspection. The raw data spectrum for a single 5 m × 5 m pixel was extracted, converted to radiance using the laboratory calibration, and corrected to surface reflectance using MODTRAN3 within ISDAS. This procedure was repeated for the same pixel spectrum, using the set of corrected coefficients derived using the RBVC method to go from DN to radiance, which was then corrected to surface reflectance.

To compare the ground-based reflectance spectra with the recalibrated Probe-1 airborne data required an analysis of the pixel mixing effects. In linear mixture analysis (Settle & Drake, 1993), the composite reflectance spectrum $\rho(\lambda)$ can be written as a linear sum of N end member spectra, $a_n(\lambda)$, given by

$$\rho(\lambda) = \sum_{n=1}^{N} f_n a_n(\lambda) + \phi, \tag{3}$$

which is constrained by

$$\sum_{n=1}^{N} f_n = 1.0, \qquad \text{and } f_n \gtrsim 0.0 \tag{4}$$

In (3) and (4), f_n represents the fractional abundance for the nth end member, and ϕ provides a measure of the error in the unmixing. For this study, the Probe-1 mixed pixel spectrum is simulated by summing together the corrected and resampled mean field spectra of white bean leaves and soil, which are treated here as end member spectra a_1 and a_2. Then the resulting mixed spectrum is compared with the Probe-1 reflectance spectra for the same target, to validate

the corrected radiometric coefficients Note that this mixed pixel spectrum will provide a first-order approximation to the spectrum that the Probe 1 will measure, since the effects of shadow have not been included This shadow would have the greatest effect in the visible region

In the upper panel of Fig. 9, the corrected and resampled GER3700 field reflectance spectra for the bean leaves and dry soil are illustrated The mixed spectrum was created using fractions of $f_1 = 0.65$ (beans) and $f_2 = 0.35$ (soil), which are consistent with the crop coverage as estimated in the field. With respect to the bean spectrum, mixing with the parched soil spectrum has the effect of increasing the reflectance in the SWIR, decreasing the chlorophyll absorption at 680 nm, and decreasing the reflectance in the NIR

In the lower panel of Fig 9, the Probe 1 reflectance spectrum for the mixed pixel, illustrated with both the laboratory and the corrected coefficients, is compared with mixed spectrum derived from the field spectra It is immediately obvious that the corrected Probe 1 spectrum provides a much better match than using the original coefficients the relative amplitude between the peak at 850 nm and that at 1100 nm is a close match, as is the spectral shape in the vicinity of the leaf liquid water content (970 and 1180 nm) In addition, the overall shape of the corrected Probe 1 spectrum is better throughout the NIR, and it is broader in the 1500- to 1800-nm range of the SWIR, and therefore provides a better match to the mixed pixel spectrum

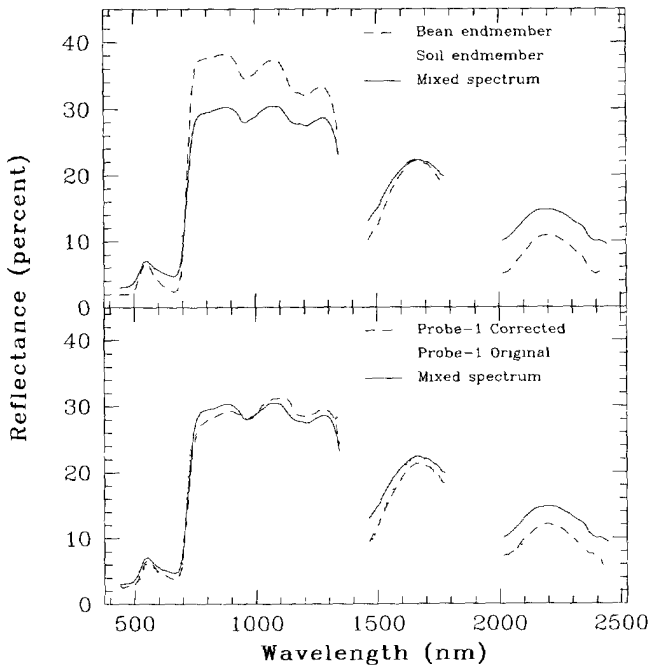

Fig 9 (Upper panel) Spectrum for a mixed pixel (solid line) simulated by summing a bean leaf spectrum ($f_1 = 0.65$) with a soil spectrum ($f_1 = 0.35$) (Lower panel) Comparison of Probe 1 reflectance spectra with the mixed pixel spectrum derived in the upper panel

This construction of a composite spectrum from GER3700 end member spectra and its comparison with the airborne Probe 1 reflectance spectrum is a straight forward analysis that illustrates using independent data that the RBVC method was successful in correcting the radiometric coefficients The primary discrepancy between the corrected Probe 1 spectrum and the mixed field spectrum is visible in the lower panel of Fig 9, where the amplitudes of the Probe 1 spectra in the SWIR are ≤3% lower than that of the mixed field spectrum This can be explained by higher moisture content in the shaded soil as compared to the dry soil used to construct the mixed field spectrum.

5. Error analysis and budget

The reflectance spectra based upon the corrected radiometric coefficients and plotted in Figs 7–9 are free of the obvious problems visible in the original data. However, their accuracy remains to be assessed Here, the total uncertainty inherent in the reflectance spectra is evaluated by estimating the uncertainty arising due to each component of the RBVC method. For the most part these uncertainties vary with wavelength, and for the purpose of providing a single representative value, the full wavelength range has been divided into its VNIR and SWIR components, and the uncertainties are averaged across these ranges These uncertainties are given as percent relative error together with the total RMS uncertainty for each wavelength region

(a) Radiance measurements of the calibration target are converted to reflectance spectra using reference scans of a Spectralon panel The uncertainty associated with each field reflectance spectrum measurement is due to *corrections for spectral and angular variations in reflectance of the Spectralon panel*, as described in Section 2. The scatter in the measured correction factors about the interpolating polynomial function (Fig 1) give rise to an uncertainty of about 1.0% in both the VNIR and SWIR ranges.

This is the total contribution to the error budget directly associated with the GER3700 field spectrometer, assuming as we have that errors due to device linearity and stability are not manifest here These are valid assumptions While the PbS detectors in the GER3700 are not stable across temperature changes, all of the measurements described in this analysis were made within a few minutes of measurement of the reference panel, which is a period of time over which the temperature remained constant As well, the Si and PbS semiconductor devices are known to be highly linear over the range of reflectances measured in this study

(b) The uncertainty on the mean field reflectance spectrum is due to *variability in the surface characteristics of the airstrip, over the region sampled during the field measurement process* This uncertainty is estimated by calculating the standard error of the mean (Section 2) at each band for the mean field reflectance spectrum Averaging over wave-

length yields relative errors of ≃4.0% in the VNIR and 3.7% in the SWIR for the Probe 1 data, and ≃1.3% for the *casi* data

(c) The inability to correlate the location of the field measurements with individual pixels in the hyperspectral scene contributes a significant uncertainty to the overall error budget, due to *inhomogeneity across the region of the hyperspectral scene used to extract spectra* for the calibration As described in Sections 4 2 and 4 3, multiple sets of corrected radiometric coefficients were derived using adjacent subregions within the visually located target sites, and used to deduce the standard error on the average values for the corrected coefficients of both hyperspectral sensors

For the Probe 1 data, a value of ≃1 5% relative error is an appropriate average over the entire wavelength range, for which the standard error varies between about 0 8% and 2 1% For the *casi* data, an appropriate average value is ≃0 7%, where the standard error varies between about 0.4% and 0 9% While these uncertainties are lower than those described in (a) and (b), they are still significant (Table 3)

(d) The MODTRAN3 RT code together with the ISDAS LUT approach (Staenz & Williams, 1997) is used to convert the hyperspectral at-sensor radiance spectra to surface reflectance (Section 3.2), and it introduces an additional source of error and a significant uncertainty Often, comparison of the atmospherically corrected reflectance spectrum with a ground-based reflectance spectrum is used to assess the accuracy of the RT code (Green et al , 1996, Staenz & Williams, 1997). In this case, however, the ground-based reflectance spectrum is used as an input to the RBVC method and so cannot be used to assess these uncertainties.

The atmospheric correction process includes many sources of error, including uncertainties in the RT code, such as (1) uncertainty in the exoatmospheric solar irradiance spectrum, (2) use of standard models for the gaseous and haze components of the atmosphere in place of measured atmospheric parameters (e g., radiosonde data), (3) approximations in the atmospheric physics used to model the scattering and absorption processes, (4) BRF effects of the target in the hyperspectral scene As well, there are uncertainties in application of the atmospheric correction procedure used for this study, such as (1) the linear interpolation between breakpoints of the LUT, (2) the parametric equations used to convert the at-sensor radiance to surface reflectance, (3) estimation of the atmospheric water vapour content (U_{H_2O}) from the hyperspectral data

To identify all and assess the significance of these uncertainties is far too complex, a discussion of some of these effects is found in Slater et al (1996). Instead, reference is made to previous studies that have assessed the accuracy of the atmospheric-correction process via a controlled comparison with ground-based data. Typical relative uncertainties derived by Staenz & Williams (1997) and Green et al. (1996) are on the order of 3 5%, averaged over the full wavelength range This number includes all aspects of the uncertainties in the RT codes and LUT approach, and include some of the uncertainties associated with the acquisition of the field reflectance spectra For this study, the value of ≃3.5% is adopted as an upper limit to the relative uncertainty associated with the atmospheric correction procedure

(e) Within the vicarious calibration process, the radiometric coefficients of the hyperspectral data are adjusted until the airborne reflectance spectrum matches the mean ground-based reflectance spectrum to within a matching tolerance For both the Probe 1 and *casi* data sets, this tolerance was set to an absolute value of 0 02% absolute reflectance. For the Raglan calibrating spectrum (Fig 4), this corresponds to a relative error of ≃0 14% in the VISNIR and ≃0 12% in the SWIR For the Goose Bay calibrating spectrum (Fig 5), this corresponds to a relative error of ≃0 13% in the VISNIR Uncertainties at these levels are negligible compared to that introduced by the sources of error described in (a) through (d)

The sources of error described in (a) through (e) are added together in quadrature to yield the total RMS relative uncertainty for each wavelength region These are summarised in Table 3 For the Probe 1 data, this uncertainty is ≃5 6% in the VNIR and ≃5 4% in the SWIR For the *casi* data, the total RMS uncertainty is ≃3 9% averaged over the VNIR.

Table 3
Error budget for the vicarious calibration of the Probe 1 (Raglan) and the *casi* (Goose Bay) hyperspectral data sets

	Relative error (%)		
	Probe 1		*casi*
Type of uncertainty	VNIR	SWIR	VNIR
Interpolation of correction factors for Spectralon panel	1 0	1 0	1 0
Standard error of mean GER3700 reflectance spectrum used for calibration	4 0	3 7	1 3
Spatial registration of calibration site	1 6	1 6	0 75
Atmospheric correction process	3 5	3 5	3 5
Total RMS uncertainty	5 6	5 4	3 9

The relative error is an average over the specified wavelength range

6. Discussion

The RBVC method as applied in this paper provides a fast and powerful technique for correcting the radiometric coefficients — or to perform a radiance renormalisation - -

of airborne hyperspectral data. When applied in the operational setting of northern Canada, the RBVC method yields corrected coefficients and final reflectance spectra that are sufficiently accurate for further analysis. The coefficients corrected via the RBVC method can then be used to convert the raw hyperspectral data (DN) to radiance for any other flight line, independent of the atmospheric conditions, solar zenith or azimuth angles, terrain elevation or sensor altitude, as long as the instrument remains stable.

For the Raglan and Goose Bay projects, the total RMS uncertainties (relative) are in the range of 3.9–5.6%. Significant components of the total uncertainty are due to the field measurement of the calibration target with the GER3700 spectrometer, and its registration within the hyperspectral scene. These uncertainties can be reduced if:

(1) The number of field measurements made within the target area are increased.

(2) A calibration target is used that is as large and homogeneous as possible, and an accurate location for each of the field measurements is determined as accurately as possible, in a manner that will permit accurate registration, on an individual pixel level, within the hyperspectral scene. As well, given the choice of targets in a specific field environment, a brighter target is preferred over a darker target since its reflectance spectrum will have a higher signal-to-noise ratio.

(3) Field measurements are obtained for $N > 1$ calibration sites within the flight line. These multiple sites can be used independently to derive corrected radiometric coefficients, so that the uncertainties on the final averaged coefficients are reduced by a factor of $\sqrt{N}$.

7. Conclusions

The RBVC method provides a fast and powerful technique for correcting the radiometric coefficients – or to perform a radiance renormalisation — of airborne hyperspectral data in operational settings. If the hyperspectral overflights are supported by field measurements of reflectance spectra, then it is a minimal additional effort to locate and measure a homogeneous target within the overflight area. This provides the data necessary to check the radiometric calibration, and to correct the coefficients using the RBVC method if necessary. The RBVC method was implemented in ISDAS as an iterative numerical technique that utilizes the MODTRAN3 radiative transfer code to atmospherically correct the at-sensor hyperspectral data to surface reflectance, and then adjusts the radiometric coefficients until the two spectra match within a tolerance of 0.02% absolute reflectance at every band. The coefficients corrected via the RBVC method can then be used to convert the raw hyperspectral data (DN) to radiance for any other flight line, independent of the atmospheric conditions, solar zenith or azimuth angles, terrain elevation or sensor altitude. For this study, the total relative errors are in the range of 3.9–5.6%, and the validity of the RBVC has been verified using independent field measurements.

Acknowledgments

The authors wish to thank J. Gingerich (Noranda Mining and Exploration) and R. Moore (Falconbridge) for making the Probe 1 data over the Kattiniq/Donaldson airstrip available to CCRS. Thanks to M. Peshko (Noranda Mining and Exploration), and L. McBean and J. Wong (Falconbridge) for their technical support. As well, we would like to thank R. Neville, D. Hodgson, F. Vachon and J.-C. Deguise for their comments and assistance. The authors acknowledge the financial support of Barrick Gold, Cameco, Cominco, De Beers Consolidated Mines, Falconbridge, Noranda Mining and Exploration, and Placer Dome Exploration.

References

Anderson, G. P., Wong, J., & Chetwynd, J. H. (1995). MODTRAN3: an update on recent validations against airborne high resolution interferometer measurement. *Summaries of the fifth annual JPL airborne earth science workshop. Jet Propulsion Laboratory, Pasadena, USA. JPL Publication 95-1* (Vol. 1, pp. 5–8).

Anger, C. D., Achal, S., Ivanco, T., Mah, S., Price, R., & Busler, J. (1996). Extended operational capabilities of CASI. *Proceedings of the second international airborne remote sensing conference, San Francisco, CA* (pp. 124–133).

Babey, S. K., & Anger, C. D. (1989). A compact airborne spectral imager (SASI). *Proceedings of the IGARSS'89 twelfth Canadian symposium on remote sensing, Vancouver, Canada. IEEE* (Vol. II, pp. 1028–1031).

Berk, A., Bernstein, L. S., Robertson, D. C. (1989). *MODTRAN: a moderate resolution model for LOWTRAN7*. Final Report, GL-TR-0122, AFGL, Hanscom AFB, MD.

Dinguirard, M., & Slater, P. N. (1999). Calibration of space-multispectral imaging sensors: a review. *Remote Sensing of Environment, 68*, 194–205.

Gao, B.-C., & Goetz, A. F. H. (1990). Column atmospheric water vapour and vegetation liquid water retrievals from airborne imaging spectrometer data. *Journal of Geophysical Research, 95* (D4), 3549–3564.

Green, R. O., Conel, J. E., Margolis, J. S., Bruge, C. J., & Hoover, G. L. (1991). An inversion algorithm for retrieval of atmospheric and leaf water absorption from AVIRIS radiance with compensation for atmospheric scattering. *Proceedings of the third JPL airborne earth science workshop. Pasadena, CA. JPL Publication 91-28* (Vol. 1, pp. 51–61).

Green, R. O., Conel, J. E., Margolis, J. S., Chovit, C., & Faust, J. (1996). Inflight calibration and validation of the airborne visible/infrared imaging spectrometer (AVIRIS). *Proceedings of the sixth JPL airborne earth science workshop. Pasadena, CA. JPL Publication 96-4* (Vol. 1, pp. 115–126).

Markham, B., Barker, J., Slater, P. N., & Biggar, S. (1997). Radiometric calibration of Landsat. *Photogrammetric Engineering and Remote Sensing, 63*, 853–858.

Neville, R. A., Rowlands, N., Marois, R., & Powell, I. (1995). SFSI: Canada's first airborne SWIR imaging spectrometer. *Canadian Journal of Remote Sensing, 21*, 449–456.

Pollock, P. L., Beauchemin, M., Fedosejevs, G., Fung, K. B., Gauthier, R. P., Pan, D., & Whitney, A. L. (2000). Use of remote sensing generated landscape metrics for environmental monitoring in Labrador, Canada. *Fourth international conference on integrating GIS and environmen-*

tal modelling measurement (including data) and indicators, Alberta, Canada (Paper published and available from (http://www.colorado.edu/research/cires/banff/upload/172/))

Settle, J. J., & Drake, N. A. (1993). Linear mixing and the estimation of ground cover proportions. *International Journal of Remote Sensing, 14*, 1159–1177.

Slater, P. N., Biggar, S. F., Holm, R. G., Jackson, R. D., Mao, Y., Moran, M. S., Palmer, J. M., & Yuan, B. (1987). Reflectance- and radiance-based methods for the in-flight absolute calibration of multispectral sensors. *Remote Sensing of Environment, 22*, 11–37.

Slater, P. N., Biggar, S. F., Thome, K. J., Gellman, D. I., & Spyak, P. R. (1996). Vicarious radiometric calibration of EOS sensors. *Journal of Atmospheric and Oceanic Technology, 13*, 349–359.

Staenz, K., Nadeau, C., Secker, J., & Budkewitsch, P. (2000). Spectral unmixing applied to vegetated environments in the Canadian Arctic for mineral mapping. *Proceedings of the XIXth ISPRS congress, Amsterdam the Netherlands. International Archives of Photogrammetry and Remote Sensing*, 1464–1471.

Staenz, K., Szeredi, T., & Schwarz, J. (1998). ISDAS — a system for processing/analyzing hyperspectral data. *Canadian Journal of Remote Sensing, 24*, 99–113.

Staenz, K., & Williams, D. J. (1997). Retrieval of surface reflectance from hyperspectral data using a look-up table approach. *Canadian Journal of Remote Sensing, 23*, 354–368.

Teillet, P. M., Slater, P. N., Ding, Y., Santer, R. P., Jackson, R. D., & Moran, M. S. (1990). Three methods for the absolute calibration of the NOAA AVHRR sensors in-flight. *Remote Sensing of Environment, 31*, 105–120.

Thome, K., Arai, K., Hook, S., Kieffer, H. Lang, H., Matsunaga, T., Ono, A., Palluconi, F., Sakuma, H. Slater, P. N., Takashima, T., Tonooka, H., Tsuchida, S., Welch, R. M., & Zalewski, E. (1998). ASTER preflight and inflight calibration and the validation of level 2 products. *IEEE Transactions on Geoscience and Remote Sensing, 36*, 1161–1172.

Thome, K., Markham, B., Barker, J., Slater, P. N., & Biggar, S. (1997). Radiometric calibration of Landsat. *Photogrammetric Engineering and Remote Sensing, 63*, 853–858.

Vane, G., Green, R. O., Chrien, T. G., Enmark, H. T., Hansen, E. G., & Porter, W. M. (1993). The airborne visible/infrared imaging spectrometer (AVIRIS). *Remote Sensing of Environment, 24*, 127–143.